Geophysical Journal International

Geophys. J. Int. (2016) **204,** 907–917
GJI Seismology

doi: 10.1093/gji/ggv454

Subsurface fluid distribution and possible seismic precursory signal at the Salse di Nirano mud volcanic field, Italy

Matteo Lupi,[1] Barbara Suski Ricci,[2] Johannes Kenkel,[3] Tullio Ricci,[4] Florian Fuchs,[5] Stephen A. Miller[6] and Andreas Kemna[3]

[1] *Department of Earth Sciences, University of Geneva, Geneva, Switzerland. E-mail: matteo.lupi@unige.ch*
[2] *MEMSFIELD, Clamart, France*
[3] *Department of Geophysics, Steinmann Institute, Bonn University, Bonn, Germany*
[4] *Istituto Nazionale di Geofisica e Vulcanologia, Rome, Italy*
[5] *Department of Meteorology and Geophysics, University of Vienna, Vienna, Austria*
[6] *Centre for Hydrogeology and Geothermics, University of Neuchatel, Neuchatel, Switzerland*

Accepted 2015 October 16. Received 2015 October 16; in original form 2014 October 3

SUMMARY

Mud volcanoes are geological systems often characterized by elevated fluid pressures at depth deviating from hydrostatic conditions. This near-critical state makes mud volcanoes particularly sensitive to external forcing induced by natural or man-made perturbations. We used the Nirano mud volcanic field as a natural laboratory to test pre- and post-seismic effects generated by distant earthquakes. We first characterized the subsurface structure of the Nirano mud volcanic field with a geoelectrical study. Next, we deployed a broad-band seismic station in the area to understand the typical seismic signal generated by the mud volcano. Seismic records show a background noise below 2 s, sometimes interrupted by pulses of drumbeat-like high-frequency signals lasting from several minutes to hours. To date this is the first observation of drumbeat signal observed in mud volcanoes.

In 2013 June we recorded a M4.7 earthquake, that occurred approximately 60 km far from our seismic station. According to empirical estimations the Nirano mud volcanic field should not have been affected by the M4.7 earthquake. Yet, before the seismic event we recorded an increasing amplitude of the signal in the 10–20 Hz frequency band. The signal emerged approximately two hours before the earthquake and lasted for about three hours. Our statistical analysis suggests the presence of a possible precursory signal about 10 min before the earthquake.

Key words: Tomography; Gas and hydrate systems; Earthquake interaction, forecasting, and prediction; Seismicity and tectonics; Volcano seismology; Mud volcanism; Europe.

1 INTRODUCTION

Mud volcanism is recognized around the globe with examples from Trinidad, USA, Azerbaijan, Pakistan, China, Java and Italy. These geological systems originate as consequence of fast depositional processes occurring in convergent margins, tectonic belts, submarine slopes, and more generally, where the elevated sedimentation rate impedes fine sediments to dehydrate before being buried. This allows fluids to be retained at depth promoting the formation of isolated geological compartments with elevated fluid pressures. The proximal region of the Northern Apennines, immediately South of the Pede-Apennines thrust, North Italy, is characterized by several mud volcanic systems aligned along a narrow WNW-ESE trending region that runs subparallel to the Pede-Apennines thrust (Fig. 1a).

The Nirano mud volcanic field (NMVF) is located approximately 20 km SW of Modena, Italy, and sits upon an anticline structure with a NW–SE axis associated to the Pede-Apennines thrust (Bonini 2008). The geological sequence below the NMVF (from depth to surface) consists of Miocene Marnoso Arenacea formations (sandstones and siltstones) at approximately 2 km depth, overlayered by the Ligurian (shales) and the Epi-Ligurian Units (sandstones, clays stones and conglomerates). The latter are covered by the gently folded silty clays formations (Argille Azzurre) dating from Middle Pliocene to Lower Pleistocene. Bonini (2008) suggests that the NMVF is fed by deep fluids (seeping from the Marnoso Arenacea formation) upwelling along high-angle thrust faults. Fluids accumulate in shallow reservoirs at approximately 0 m a.s.l. within the permeable Epi-Ligurian Units, which are capped by low permeability clays. From here fluids migrate vertically through the Marine clays and silty clays reaching the surface at the NMVF.

Fig. 1 shows the main geological features of the region, including the distribution of the mud volcanic centres and an aerial view of the NMVF. The NMVF consists of four main emission centres (cones or 'salse') aligned along a N55 direction (Fig. 2). Each emission centre is subcircular in shape, with a radius of about 20 m, and may reach up to 3 m above the ground. The cones consist of one or more mud vents

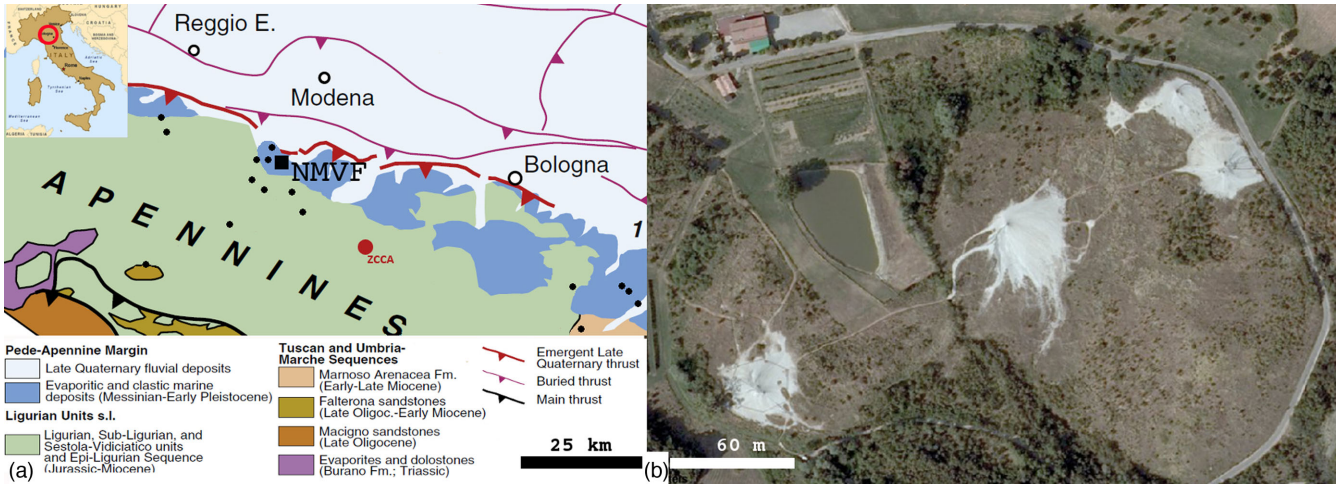

Figure 1. Geological map of the Pede-Apenninic region. Black dots show the location of the mud emissions occurring in the Pede-Apennine margin and the black square points out the location of the Nirano mud volcanic field and NIR seismic station. The red circle shows the location of ZCCA seismic station. The Pede-Apeninne thrust is marked by the bold red line on the left. Modified after Bonini (2012).

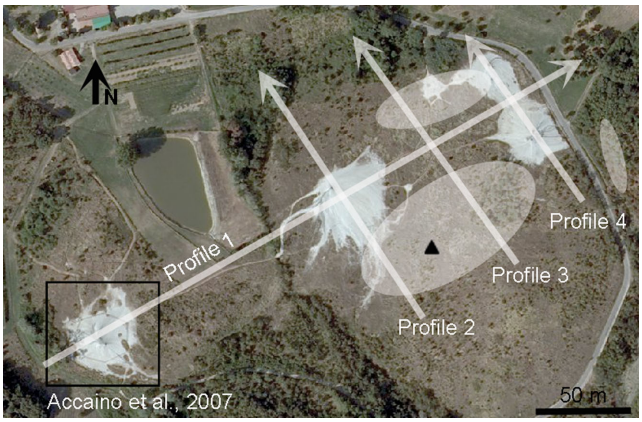

Figure 2. Top view of the Nirano mud volcanic field showing the four main mud volcanic emission centres. The white arrows indicate the direction and the length of the geoelectrical profiles presented in this work, the black triangle indicates the position of the seismic station. White shaded areas indicate regions characterized by the expulsion of mud after the 2012 Emilia seismic sequence while the black square points out the region investigated by Accaino *et al.* (2007).

and the expulsion of fluids is rhythmic and regular within a narrow time window (i.e. from hours to days). The mud cones are hosted in a subsided area that is morphologically similar to a volcanic caldera. Bonini (2008) suggests that the expulsion of thousands of cubic metres of mud over the centuries may have induced subsidence and compaction of the shallower structural levels, promoting the formation of the subsided area.

Onset of mud volcanism is often related to seismic activity, with many examples of earthquakes affecting or triggering mud volcanoes (e.g. Mellors *et al.* 2007; Manga *et al.* 2009; Lupi *et al.* 2013). Martinelli & Ferrari (1991) highlight that the normal activity of some mud system in northern Italy is periodically interrupted by paroxysmal events. Bonini (2009) points out that the NMVF showed a remarkable increase of fluid emission after the 1873 May 15 earthquake that occurred at the Pede-Apennines margin, near Reggio-Emilia (Fig. 1). In addition, Bonini (2008) reports of a large mud eruption that Plyni describes with sky-scraping flames and smoke visible from approximately 10 km far (Jones 2001). According to the Italian catalogue of historic seismic events (Guidoboni 1989) an earthquake occurred in 91 B.C. close to Modena and hence Plyni's observations may be related to such event.

In October 2012 we conducted a geological field survey of the NMVF observing that after the Emilia seismic sequence, that began on the 2012 May 20 (Pondrelli *et al.* 2012), new mud centres in shape of mud ponds, surface mud flows and mud-filled cracks cropped out within the NMVF. Interestingly, mud outcomes also occurred outside the subsided area that is thought to limit the mud volcanic caldera (Bonini 2008). Manga & Bonini (2012) report that the Regnano and Puianello mud volcanic centres, NW and SE of NMVF, respectively, as well as the NMVF responded to the strongest aftershocks of the Emilia seismic sequence with vigorous mud emissions. Furthermore, local foresters confirmed that the activity of the NMVF was particularly intense before the main shock of the Emilia sequence in 2012. A forester of the natural park of the NMVF was close to one of the cones when the M5.3 Lunigiana earthquake (Samsonov *et al.* 2013) struck approximately 60 km far from the NMVF on the 2013 June 21. He witnessed the following, verbatim: *I was leading a school visit through the park when the earthquake occurred. We were standing nearby the SW mud cone and at first I felt dizzy, with a feeling of spinning head. Then I felt like being above a moving water-mattress*.

Eyewitness records are often too general and not accurate enough. To avoid qualitative descriptions and ambiguous observations (that may lead to misleading conclusions) we initiated a geophysical study of the NMVF. In the following we report the results of a geoelectrical survey conducted during 2012 November at the NMVF. Electrical resistivity tomography (ERT) has proven to be a robust and reliable tool to provide realistic, albeit strongly smoothed, images of the spatial electrical resistivity distribution in the shallow subsurface (e.g. Binley & Kemna 2005). As a consequence, ERT methods have been successfully applied to a large variety of problems such as hydrogeological and environmental studies (e.g. Revil *et al.* 2012, Singha *et al.* 2015), characterization of tectonically active areas (Caputo *et al.* 2003; Nguyen *et al.* 2007; Vanneste *et al.* 2008; Suski *et al.* 2010), and most importantly in the given context, to the characterization of mud volcanoes (Istadi *et al.* 2009; Zeyen *et al.* 2011; Bessonova *et al.* 2012).

We also show results from a seismic experiment aimed at understanding the effects of regional earthquakes on the NMVF, and more generally at mud volcanoes. For this scope, we deployed a

broad-band seismic station (NIR) within the NMVF (Fig. 2). The experiment began in 2012 October and was concluded in 2013 October (more precisely from the 2012 October 16 to the 2012 November 1 and from the 2013 June 24 to the 2013 July 26). The data provide insights about the seismic signal generated (by fluids) within the NMVF. In addition, we recorded a M4.7 aftershock of the Lunigiana sequence (West of the NMVF) (Samsonov *et al.* 2013), which allowed us to describe the seismic signal recorded at the NMVF before and after the earthquake.

2 GEOELECTRICAL AND SEISMIC MEASUREMENTS

2.1 Electrical resistivity tomography

In 2012 November, we performed an ERT survey comprising several 2-D transects within the NMVF caldera to investigate the subsurface structure of this area. We acquired the geoelectrical data using a Syscal Pro multi-channel resistivity system with 48 stainless steel electrodes using dipole–dipole skip-2 and Schlumberger (gradient) configurations. The spacing between the electrodes was 5 m for the deeper profiles (Figs 3a–c) and 2 m for the shallow profile (Fig. 3d). This provided a maximum exploration depth between 20 and 50 m (mainly controlled by the length of the electrode layout). The wet season and the large amount of high-salinity fluids expelled from the mud vents provided efficient contacts between the electrodes and the ground. The white arrows in Fig. 2 show the direction of the resistivity profiles and their length. We did not perform any transverse profile across the SW cone as this was already investigated by Accaino *et al.* (2007). The longitudinal profile (Fig. 3a) is 475 m long and reaches about 50 m below the ground surface. To cover the entire longitudinal extension of the caldera we concatenated three segments to obtain a longer profile with an overlap of 24 electrodes (roll-along). The measured data were then tomographically inverted using a smoothness-constrained, Gauss–Newton-type inversion algorithm to obtain the spatial distribution of the electrical resistivity in the subsurface. Here we used the finite-element-based code CRTomo (Kemna 2000) which computes the smoothest model that explains the data within predefined error bounds. Appropriately adjusting the error model that describes data uncertainty in the inversion (e.g. Koestel *et al.* 2008) is important to avoid overfitting the data and thus the creation of artefacts in the obtained images. From a careful analysis of the data and the inversion results obtained for different error model parameters, we set the data error to a combination of 2 per cent relative and 5×10^{-4} Ω absolute resistance error. However, slightly changing these values had no noteable effect on the inversion results. Exemplary raw data are shown in Fig. 4(a) for the longitudinal profile, along with the data predicted by the inverted model and the obtained error-weighted misfit between measured and predicted data (Figs 4b and c, respectively).

2.2 Deployment of the broad-band seismic station

The black triangle in Fig. 2 indicates the position of the seismic station deployed in the NMVF. We used a Trillium 240 s broad-band

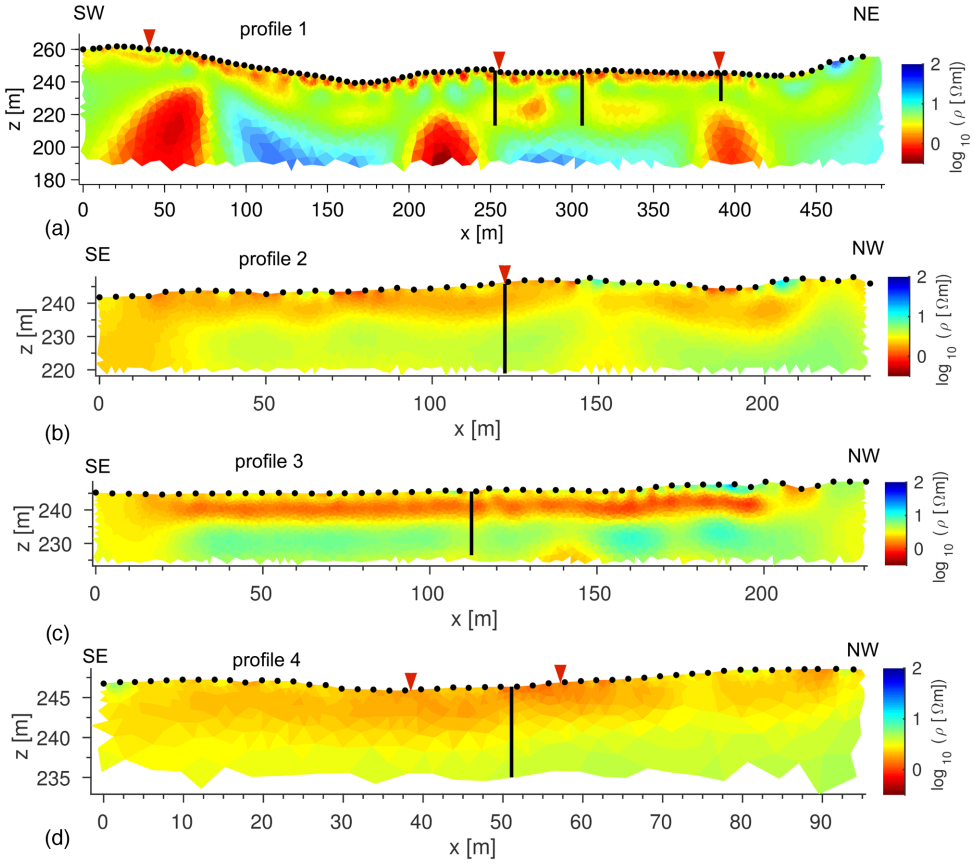

Figure 3. Inversion results of the ERT survey. (a) Profile 1, (b) Profile 2, (c) Profile 3 and (d) Profile 4. Refer to Fig. 2 for the direction of the profiles. Black lines represent the intersection between longitudinal and transverse profiles. Black dots indicate position of electrodes. The electrode spacing is 5 m in panels (a), (b) and (c) and 2 m in panel (d). Red triangles indicate the location of the mud cones and black vertical lines indicate the intersection between the profiles.

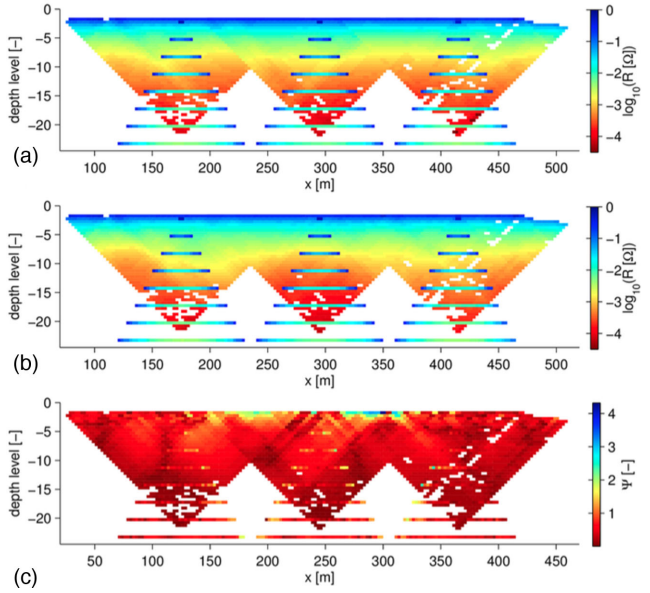

Figure 4. ERT raw data and fitting quality. (a) Pseudo-section of measured resistance data, comprising dipole–dipole (skip-2) configurations overlaid by Schlumberger (gradient) configurations, for the longitudinal ERT profile from which the inversion result in Fig. 5(a) was obtained. (b) Predicted resistance data computed from the inversion result in Fig. 5(a). (c) Error-weighted misfit, Ψ, between measured (a) and predicted (b) *log* resistance data. The value of Ψ expresses the misfit between individual measured and predicted *log* resistance data in terms of the respective standard deviation assumed as measurement error in the inversion. The data were fitted to an overall root-mean-square (rms) value of Ψ of 1.

station (sampling rate 100 Hz) equipped with a three-channel Reftek 130 data-logger to acquire the data. We used the ObsPy toolbox (Beyreuther *et al.* 2010) to process the seismic records. The station was buried 1 m deep, thermally insulated and installed on a concrete plate as no in-place rock crops out within the NMVF. This may affect the amplitude of the recorded seismic signal introducing errors on the estimation of the dynamic stress and strain associated to the passage of the seismic waves. For this reason we do not attempt any estimation of the dynamic stress associated to the passing seismic waves but we limit our observations to a descriptive approach.

3 RESULTS

3.1 Geoelectrical observations

Fig. 3 shows the results of the tomographic inversions of the geoelectrical profiles acquired within the NMVF. In the near-surface zone (approx. 0–10 m depth), the lowest resistivities (red and yellow regions indicate resistivities below 3 Ωm) correspond well with the presence of active vents (marked by red inverted triangles in Fig. 3). Measured resistivity values of the fluids inside the cones were about 0.7 Ωm, in agreement with the recovered lowest resistivity values in the electrical images (note that the images in Fig. 3 show log_{10} values of resistivity in Ωm). At intermediate depths (10–20 m), all profiles show intermediate resistivities between 3 and 10 Ωm. This suggests a fluid-saturated area terminating about 30 m below the ground surface (green area in Fig. 3a). Below this region the longitudinal profile (Fig. 3a) shows three conductive anomalies (red dome-like structures). At the surface the NMVF counts three main regions characterized by emission centres (Fig. 1a). The three conductive anomalies lay almost beneath the mud vents. Comparing

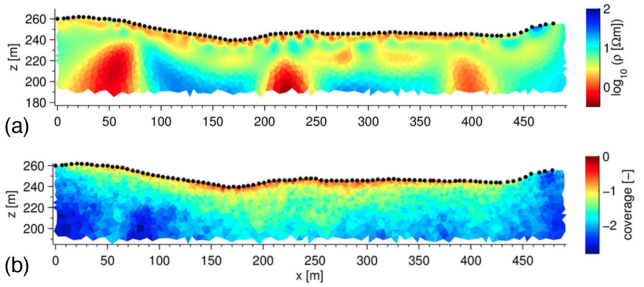

Figure 5. Inversion result and cumulative sensitivity distribution for the longitudinal ERT transect. (a) Inversion result. (b) log_{10} value of normalized cumulative (using L_1-norm) sensitivity of all inverted resistance measurements, showing how the subsurface is covered by the ERT survey. The inverted image in (a) is less controlled by the data in areas of low cumulative sensitivity (i.e. blue regions). Black dots indicate the position of the electrodes.

the imaged resistivities with those measured inside the cones at the surface suggests that in the immediate subsurface it is stored a considerable amount of (high-salinity) fluids. The fluid transfer from the fluid reservoirs to the vents at the surface may occur along narrow conduits that are beyond the resolution limits of the conducted ERT survey.

In order to assess the reliability of the recovered conductive, dome-like anomalies in the longitudinal profile, we inspected the cumulative sensitivity distribution (coverage) for the inverted data set. Additionally, we conducted a synthetic study using the same measurement geometry and configurations as in the field. Fig. 5 shows that although the recovered conductive anomalies are located at depth, where ERT sensitivity and resolution is decreased, in particular the anomalies in the middle and in the NE part of the profile are still characterized by cumulative sensitivity values that allow a quantitative interpretation (e.g. Kemna 2000; Nguyen *et al.* 2009). To explicitly prove that the conductive anomalies can be indeed recovered from the data, we inverted synthetic data computed from the obtained inversion result for the longitudinal profile. We artificially removed the central conductive anomaly at depth, using the same inversion procedure as for the field data. The corresponding inversion results, shown in Figs 6(a) and (b), respectively, clearly show that the deep conductive anomaly is not an inversion artefact but a result of information captured in the data.

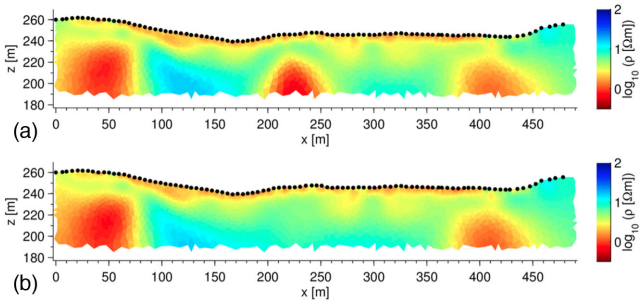

Figure 6. Synthetic ERT resolution study. (a) Result from inverting synthetic data predicted from the inverted model in Fig. 5(a). (b) Result from inverting synthetic data predicted from the inverted model in Fig. 5(a) after artificially removing the central conductive anomaly at depth. The results confirm that the central conductive anomaly is a result of information contained in the data and not an inversion artefact. Black dots indicate the position of electrodes.

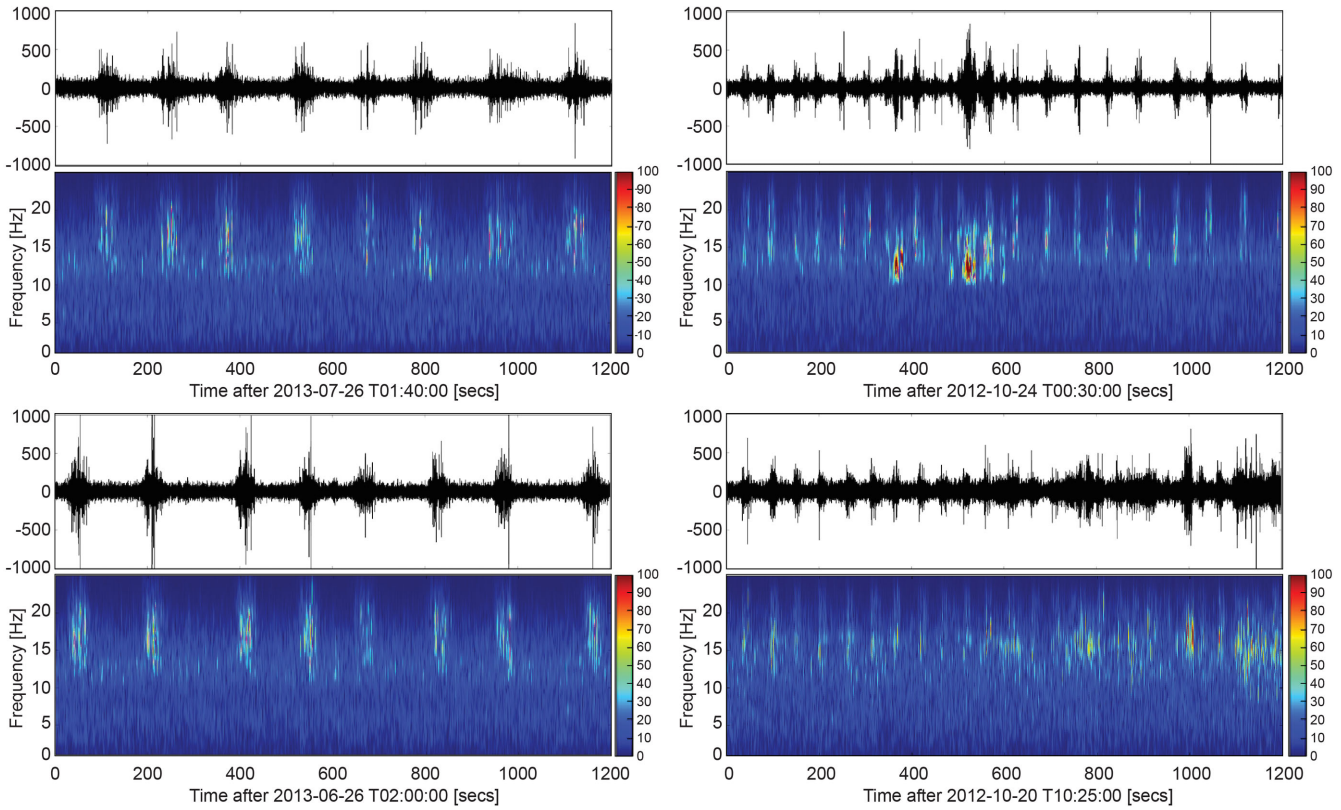

Figure 7. Waveforms of the drumbeat signal and corresponding spectrograms. The signal for the vertical component was bandpassed between 10 and 25 Hz and converted to ground velocity. The same signal also appears on the horizontal components. Note that the drumbeat signal becomes apparent only when using a high-pass filter (i.e. above 5 Hz). For the spectra presented in the manuscript we focus on the 10–25 Hz frequency band, as it is the band that best highlights the peculiar signal of the MNVF.

3.2 Seismic records

The typical seismic signal recorded by the NIR broad-band seismic station consists of background noise below 2 s, sometimes interrupted by rhythmic drumbeat high-frequency pulses lasting from several minutes to hours (Fig. 7). The drumbeat signal characterizes the higher frequencies (i.e. between 10 and 25 Hz) and appears on the three components. Each pulse lasts approximately 20 s and it is separated by intervals of low-frequency noise lasting from 40 to 180 s approximately. The time interval between two pulses is shorter in 2012 October compared to 2013 June and July, reaching *ca.* 60 s and *ca.* 100 s, respectively. We identify such a high-frequency drumbeat signal irregularly throughout our data set, with no distinction between day or night hours nor periods of the year.

In the late 2013 June the aftershocks of the M5.3 Lunigiana earthquake were still frequent (Samsonov *et al.* 2013). We recorded a M4.7 event on the June 30 (9.8 km deep), approximately 60 km South-West of the NMVF. The excitement of the lower frequencies lasted approximately 400 s, including the coda (Fig. 8). At the NMVF the earthquake caused a maximum ground velocity of approximately 3 mm s^{-1}. However, as the seismometer was deployed upon a concrete plate in soil, site effects may have altered this value.

The M4.7 earthquake allowed us to investigate the seismic behaviour of a mud volcanic system before and after a mid-size seismic event. Fig. 9 (upper row) shows the 24 hr spectrum recorded at the NIR station on the 2013 June 30, compared to a representative

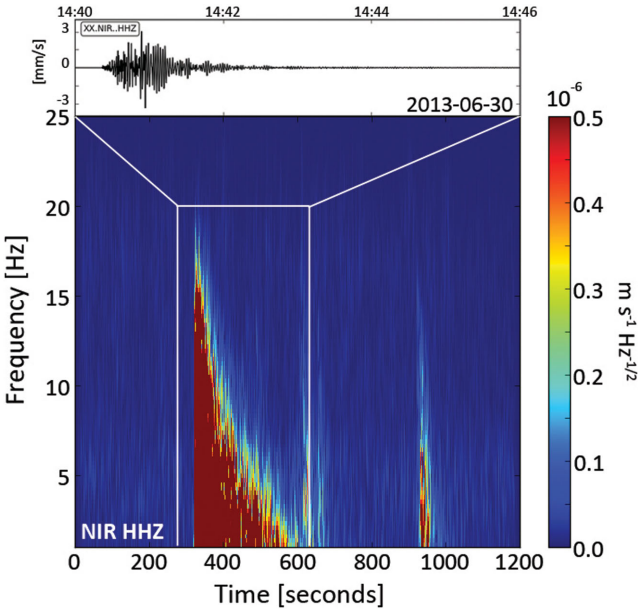

Figure 8. Spectrum and waveform of the M4.7 aftershock of the Lunigiana sequence on the 2013 June 30. The white box highlights the signature of the M4.7 earthquake. The signal around seconds 900–1000 may represent a local event near the NIR station.

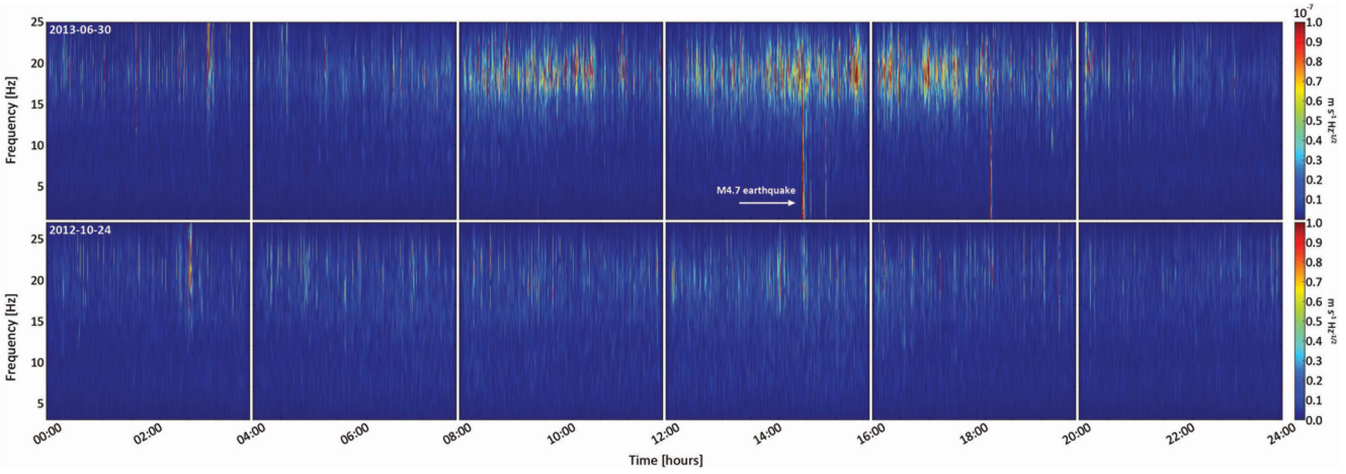

Figure 9. Spectra recorded at NIR during two different days. The upper and bottom rows show the spectra of the 2013 June 30 and 2012 October 24, respectively. Data are bandpass filtered between 10 and 25 Hz and corrected for instrument response. In the top row note the increased signal around 20 Hz lasting from approximately 12:00 UTC to 19:00 UTC and the M4.7 earthquake signature between 14:00 (UTC) and 15:00 (UTC). The bottom row is a representative example of the typical seismic signal recorded at NIR during 2012 and it does not show the noise in the high frequencies. The increased noise shown in the upper row before the earthquake is not linked to any external (artificial) source.

example (lower row) of the typical signal recorded at the NIR station. Note the increased signal around 20 Hz in Figs 9 and 10, which corresponds to the frequency band of the drumbeat signals. The excitement of the high frequencies starts at around 12:00 (UTC), increases to its peak before the earthquake (i.e. from 14:00 UTC) and lasts until about 19:00 (UTC) approximately, when the amplitude of the waveform decays.

We compared our records with other publicly available INGV seismic stations located around the NMVF finding that the excitement of the 20 Hz frequency band only occurred at the NIR seismic

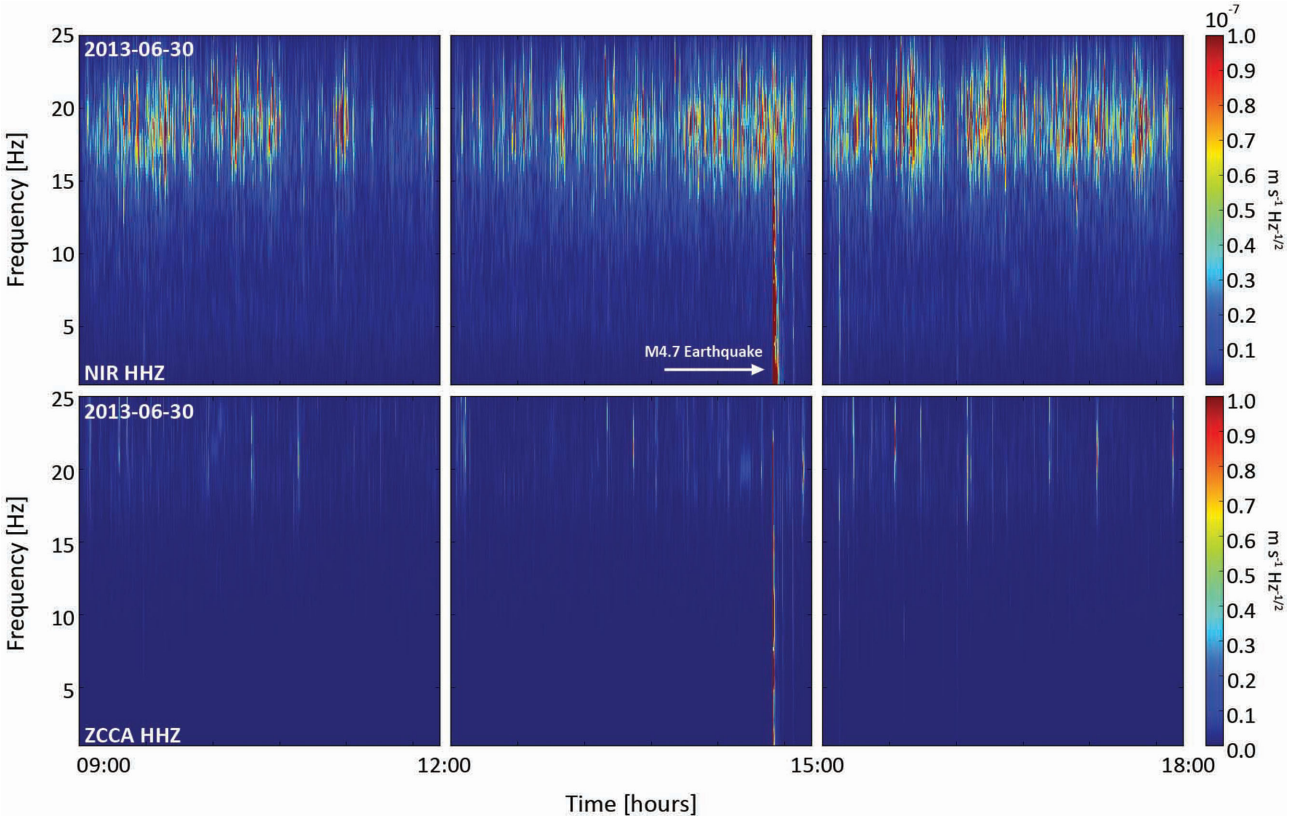

Figure 10. Seismic records of the 2013 June 30 on two different stations. Both rows show 10–25 Hz filtered and instrument corrected data before and after the M4.7 Lunigiana earthquake. The top row shows data from the NIR seismic station, while the bottom row shows data from the INGV station ZCCA (Lon: 44.35; Lat: 10.98, 22 km South-East from NIR). Note that noise level on NIR appears to increase before the marked M4.7 earthquake, while the noise level on ZCCA is low and stable.

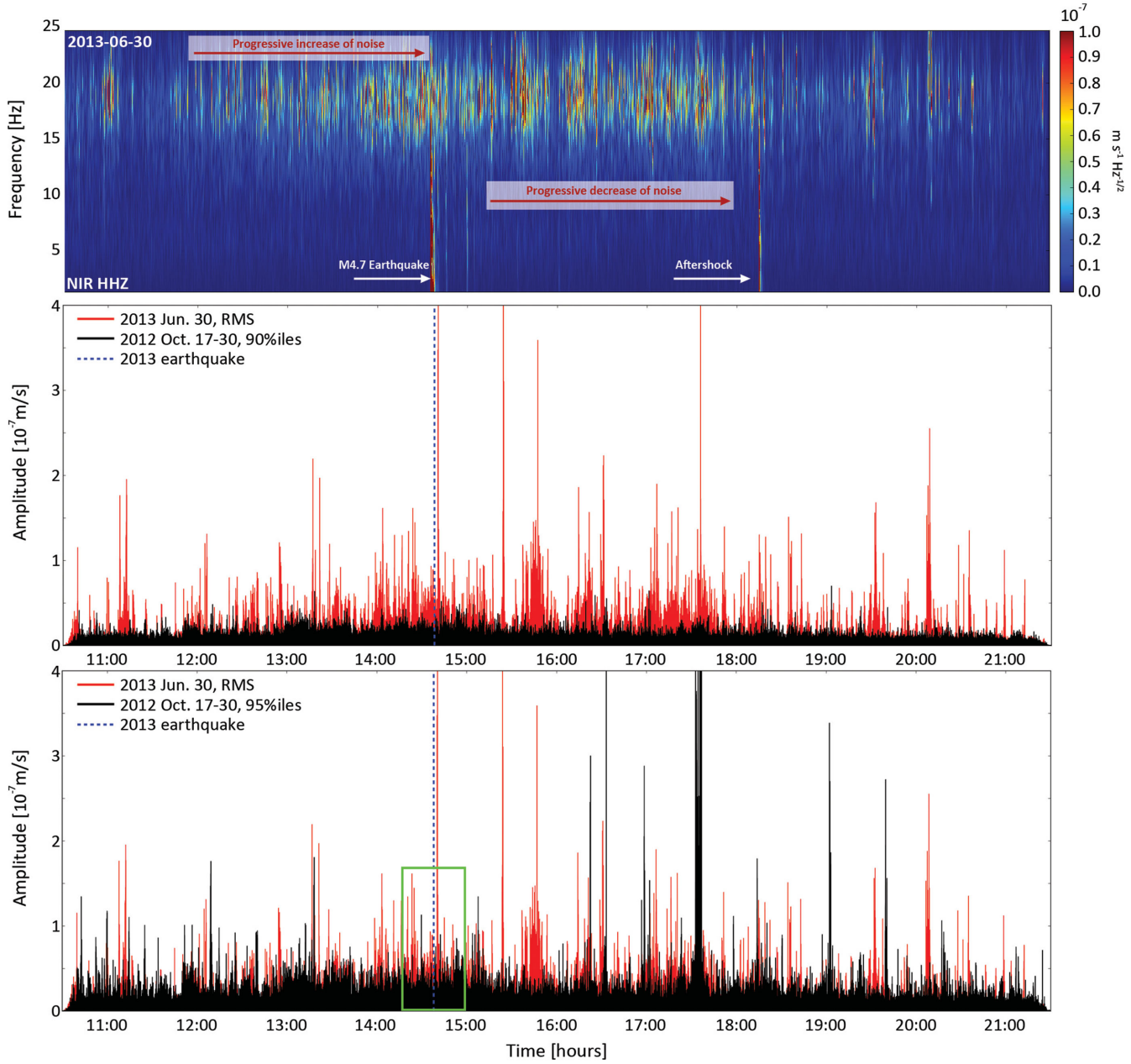

Figure 11. Spectrum and amplitude at the NIR seismic station on 2013 June 30 compared to 2012. The spectrogram on top shows instrument corrected data filtered between 10 and 25 Hz and highlights the apparent increase of noise in this frequency band before the Lunigiana earthquake. The bottom plots show root-mean-squared amplitudes of the same data (10–25 Hz filtered) on 2013 June 30 compared to the 95-percentiles and 90-percentiles of amplitudes of all available days in 2012 during the same time window. Note that the 90-percentiles of background amplitudes in 2012 are generally lower compared to 2013 June 30 and that seismic amplitudes in this 10–25 Hz band seem to increase before the 2013 Lunigiana earthquake. However, amplitudes on 2013 June 30 do not significantly exceed the 95-percentiles of data from 2012. Note that the 90-percentiles are free of high amplitude outliers such as, for example, earthquakes or other short-lived extreme values while they are still present in the 95-percentiles. The green square highlights what it is shown in Fig. 12.

station. Fig. 10 compares the signal recorded at the NIR station (upper row) with the one recorded during the same time at ZCCA station (lower row, see Fig. 1 for the location of ZCCA), about 22 km far from the NMVF. Other INGV stations nearby (e.g. NOVE, RAVA) do not show any spectra comparable to Fig. 9. This suggests that the increase of noise around 20 Hz is a local effect occurring at the NMVF. In addition, Fig. 8 shows a seismic event approximately 600 s after the arrival of the seismic waves of the M4.7 event (i.e. at around 900 s in Fig. 7). This event was not captured by nearby stations of the permanent INGV seismic network (Fig. 10) (approximately 20–30 km far from NIR) and we therefore conclude that this was a local event.

To statistically verify whether such increase of background noise may be related to the upcoming M4.7 earthquake, and therefore representing some sort of precursory signal, we inspected the spectra of the 2013 June 30 against the signal recorded at NIR station during another period. Fig. 11 compares the root-mean-squared (rms) amplitudes of ground velocity from approximately 11:00 (UTC) to approximately 21:00 (UTC) on the 2013 June 30 with the root-mean-squared amplitudes averaged over all available days in 2012

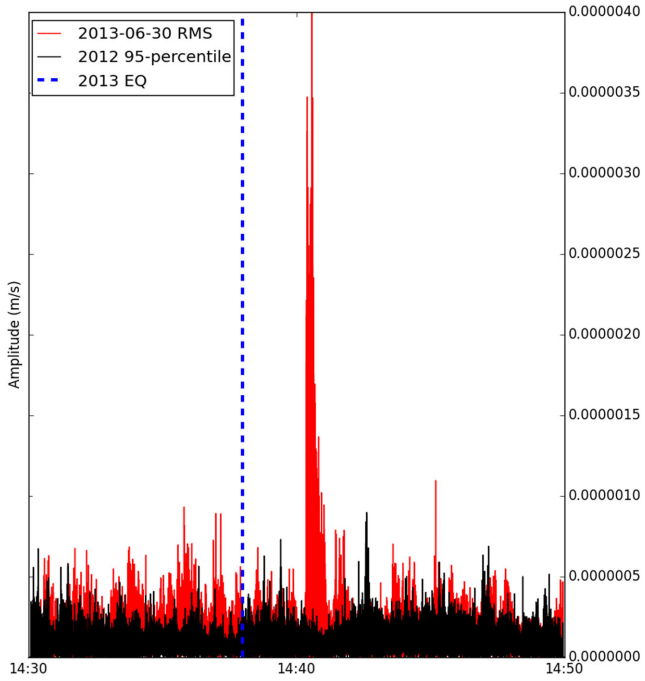

Figure 12. Close up of the root-mean-squared amplitudes shown in Fig. 11. Note the increase of amplitudes in red before and after the earthquake (blue dashed line).

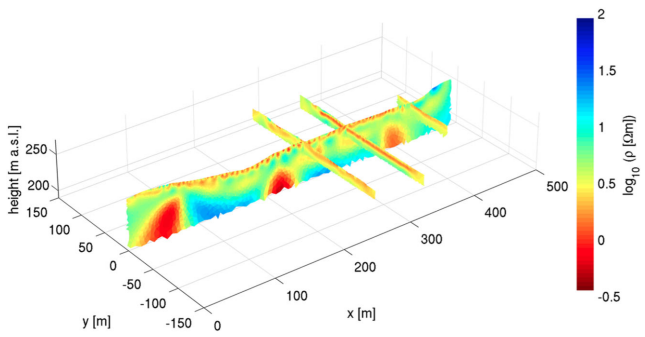

Figure 13. 3-D visualization of ERT inversion results. The transverse profiles have a lower depth of investigation due to a shorter electrode layout.

for the same time window. To verify if background rms amplitudes on 2013 June 30 significantly exceed background rms amplitudes measured during the 2012 period (implying a potential precursory signal) we calculated the 90- and 95-percentiles of amplitudes of all available data in 2012 and compared them with the amplitudes measured on 2013 June 30. We find that the long-lasting (i.e. from 12:00 to 14:30) increase of rms amplitudes before the seismic event in the 20 Hz frequency band leads to amplitudes that recognizably exceed 90 per cent of all amplitudes recorded at NIR in 2012 (Fig. 11b). However, they do not exceed the 95-percentiles of amplitudes in 2012 (Fig. 11c). However, in the minutes preceding the earthquake (i.e. about eight minutes) the amplitudes are above the 95-percentiles of amplitudes of all available data in 2012 (Fig. 12).

4 DISCUSSION

Fig. 3 shows the geoelectrical sections which exhibit visible resistivity contrasts with depth. We find a good correlation between the longitudinal and the transverse transects (Fig. 13). The shallow structure of the NMVF is characterized by low-resistivity regions that we interpret to reflect the presence of high-salinity fluids. The longitudinal profile (Fig. 3a) shows shallow, dome-like reservoirs at about 20 m below the ground surface (*ca.* 50 m wide and more than 20 m thick) feeding the mud vents. The central conductive anomaly seems to terminate towards the surface in a channel-like structure. The size of the dome structures as well as the occurrence of channel-like structures in the immediate subsurface is in agreement with previous studies (Accaino *et al.* 2007). The NE part of the NMVF is characterized by two separate mud vents (Fig. 1) that do not seem to be fed by two separate channels. Instead, the cones develop above a region characterized by a widespread distribution of fluids, which might be linked to the deeper NE reservoir (Figs 3a and d). However, given the 2-D character of the geoelectrical sections, it cannot be ruled out that also at depth a second reservoir exists outside the longitudinal image plane.

The alignment of the mud cones (Fig. 1b) suggests a N55-trending structure along which fluids reach the surface. Fluids flowing through such region reach the subsurface where they accumulate in shallow reservoirs that terminate at approximately 200 m a.s.l. (Figs 3a and 13). After the Emilia seismic sequence (Pondrelli *et al.* 2012), new isolated mud extrusions cropped out within the NMVF but also outside the areas around the mud vents. Therefore, the mud may have been extruded from the immediate subsurface that is characterized by the widespread presence of fluids. This would also explain the occasional migration of new mud centres within the subsided area that hosts the mud cones.

The drumbeat signal observed at the NMVF (Fig. 7) was previously recorded in volcanoes characterized by dome growth (e.g. St. Helens volcano, USA; Iverson *et al.* 2006). Such signal was also observed during dome extrusion at Montserrat volcano (Neuberg 2000), where with time the drumbeat signal was eventually merging together to generate continuous volcanic tremor. Iverson *et al.* (2006) suggest that in volcanic environments characterized by dome extrusion the drumbeat signal may be associated to stick-slip motion along the margins of the extruding plug. Kawakatsu *et al.* (2000) describe long-period volcanic (drumbeat) tremor at Aso volcano, Japan. In this case the long-period volcanic tremor was proposed to be generated by fluids circulating in the hydrothermal system of the Aso volcano, Japan. We suggest that the drumbeat signal sometimes observed at the NMVF may be generated by impulsive events as suggested by Kedar *et al.* (1998) for the Old Faithful Geyser in Yellowstone. Kedar *et al.* (1998) model the drumbeat signal as the collapse of a spherical bubble of gas rising through the conduit. While for the Old Faithful the occurrence of the harmonic tremor is connected to the discrete collapse of a bubble in a superheated water column, the drumbeat signal recorded at the NMVF cannot be associated to cooling dynamics as proposed by Kedar *et al.* (1998). We rather argue that the main factors controlling the rhythmicity and the lasting of each pulse are the mass flux and the geometry of the conduit. We speculate that gases released from deep reservoirs may migrate through channel-like structures or fault planes. Such fluid flow behaviour maintains the pressure high enough to support the expulsion of the hydrocarbon–mud mixture progressively reducing fluid pressure at depth. This leads to compaction of the shallows sediments, which in turn promotes the subsidence of the caldera. We exclude any anthropogenic origin (i.e. a factory or any sort of pump-induced signal) due to the varying time lag that separates each high-frequency peak throughout different pulsing events. The drumbeat signals also occur on shorter timescales (i.e. several seconds) indicating that such mechanism is a fluid flow behaviour typical of the NMVF. In addition, the NMVF is a natural reserve

and the closest (private) borehole would be more than 3 km distant. No pumps were used in the artificial lake located within the NMVF when we identified the drumbeat signal.

Figs 9–11 show that on the 2013 June 30 the seismic background level of amplitudes broadly increased before the M4.7 earthquake. Such increase results in amplitudes that exceed the 90-percentiles of the amplitudes measured in 2012 but it is comparable to the 95-percentiles of amplitudes in 2012. Only the 95-percentiles of about an hour before the M4.7 earthquake (i.e. from 14:00 p.m.) seem to exceed the amplitudes measured in 2012. The data show that the closer in time to the earthquake, the higher are the amplitudes. For instance, the amplitudes on the 2013 June 30 are higher than the 95-percentiles of amplitudes in 2012 about 10 min before the earthquake (Fig. 12). Hence, our statistical analysis suggests the presence of a possible precursory signal beginning about 10 min before the earthquake. Further studies will be necessary to validate (or disprove) our findings.

The increase of the background noise may be due to different processes. For instance, Crampin *et al.* (1984) suggest that fluid-filled microcracks and intergranular pore spaces may be reactivated before the main shock in the earthquake preparation zone. It is generally well established that fluid-saturated regions may provide more insights for the understanding of precursors of seismic events (Rice & Rudnicki 1979; Roeloffs 1988; Sammonds *et al.* 1992; Park *et al.* 1993; Chadha *et al.* 2003; Skelton *et al.* 2014). Mud volcanoes are characterized by elevated fluid pressure driving the expulsion of deep-seated fluids at the surface. We suggest that the region of the NMVF was within the earthquake preparation zone of the M4.7 earthquake. This is a reasonable assumption considering that the epicentre of the M4.7 earthquake is only 60 km far from the NMVF. In this region crustal dilation associated with stress build-up before the earthquake may have promoted a more intense release of fluids from structural regions characterized by already elevated fluid pressures at depth. This may have resulted in a more vigorous fluid flow that was captured by the NIR seismic station (Fig. 11).

During the M4.7 earthquake, the NMVF may have been affected by the elastic perturbation imposed by the main slip in the upper crust. This mechanism, normally suggested as induced in the upper plate by mega-thrust earthquakes at convergent margins (Conrad *et al.* 2004; Lupi *et al.* 2014), could also occur for intra-plate seismic events. This, combined with the dynamic stress associated to the passage of the seismic waves released by the slip, may have contributed in maintaining the elevated level of noise shown in Figs 9–11 also after the earthquake.

The frequency band between 10 and 25 Hz also shows an excitement, although decreasing with time, after the M4.7 earthquake (Fig. 11). Previous authors (Frehner & Schmalholz 2010; Korneev 2011; Maksimov *et al.* 2011) highlighted the effects generated by seismic waves propagating along fluid-filled fractures. Incident body waves may generate secondary seismic waves called Krauklis waves that may fall into resonance emitting a dominant frequency (Frehner 2014) while propagating back and forth along fluid-filled fractures. Krauklis waves may also be generated by fluid overpressure produced inside the fluid-filled fractures (Ferrazzini *et al.* 1990). Therefore, the excitement of the frequency band highlighted in Fig. 11 may be due to Krauklis waves generated by incoming seismic energy. This effect seems to be peculiar of the NMVF as the records from the publicly accessible seismic stations from the INGV network around the NMVF do not show a similar behaviour (e.g. ZCCA; Fig. 10).

In addition, the effects of the seismic waves (i.e. body waves) generated by the M4.7 earthquake at the NMVF may have been enhanced by the overall geological structure upon which the mud volcanic field resides. Similarly to the LUSI mud system, Indonesia, the NMVF sits upon a parabolic-shaped geological structure (in this case an anticline (Bonini 2008)) and may be characterized by an elevated contrast of impedances at depth. The incoming seismic energy generated by the M4.7 earthquake could have been amplified and focused by the anticline structure affecting the deep fluid reservoir. This may have led to an acceleration of the fluid flow within the high-angle thrust fault leading to the almost continuous excitement of the high frequencies shown in Fig. 11.

The M4.7 earthquake that induced the excitement of the high frequencies shown in Fig. 11 falls inside the triggering threshold for mud and magmatic volcanoes proposed by Delle Donne *et al.* (2010) and well outside the threshold proposed by Manga *et al.* (2009). Delle Donne *et al.* (2010) use a satellite-derived heat flux inventory for global volcanism to identify earthquake-induced thermal anomalies at active volcanic and mud systems. Manga *et al.* (2009) propose a large database derived from peer-reviewed literature, eyewitness observations and historical records. The most prominent difference between these two studies (and hence the triggering thresholds) resides in the choice of Delle Donne *et al.* (2010) to include measured processes that may not be directly observed at the surface. In addition to this study, we measured and investigated other instances of triggered activity (i.e. Lupi *et al.* 2013; Farias *et al.* 2014) falling outside the threshold proposed by Manga *et al.* (2009) and in agreement with Delle Donne *et al.* (2010). Our approach and findings best fit the triggering threshold proposed by Delle Donne *et al.* (2010). This points out that geophysical observations are not always in agreement with eyewitness records. Indeed, geological systems may be affected by remote earthquakes without any apparent manifestation at the surface. Note that analyzing dynamic triggering thresholds by remote earthquakes may also require to include additional parameters such as ground motion, frequency content and angle of incidence (Hill & Prejean 2007). Increasing the number of measured triggered dynamics will increase our understanding of how geological processes interact.

5 CONCLUSIONS

We have performed a resistivity study within the NMVF. Results revealed the depth of the fluid-saturated shallow region and delineated distinct dome-like shallow reservoirs. This highlighted the widespread occurrence of fluids in the subsurface that would explain the emergence of new mud centres immediately after the 2012 Emilia seismic sequence inside the NMVF.

Our study shows that the typical seismic signal recorded at the NMVF consists of background noise below 2 s, sometimes interrupted by rhythmic drumbeat-like high-frequency pulses lasting from several minutes to hours. We suggest that such pulsing events may be associated to the collapse of bubbles of gas during their ascent within the conduit from the deeply seated fluid reservoir to the fluid saturated subsurface.

An increasing amount of geophysical data point out that small magnitude seismic events may affect geological systems more than it was previously thought. In particular, this work shows that a M4.7 earthquake occurred on the 2013 June 30 approximately 60 km South-West of the NMVF may have affected the seismic signal recorded by a broad-band seismic station deployed in the mud volcanic field. This highlights that regional mid-size earthquakes may be anticipated at the NMVF by an increase of the noise level linked to fluid flow dynamics. Such behaviour could be related to the

pre-seismic stress build-up occurring around the earthquake preparation zone.

During and after the earthquake, the waves generated in the seismic slip may excite the frequency band between 10 and 20 Hz promoting the propagation of Krauklis waves. This may be accompanied by a more vigorous vertical migration of deep fluids favoured by a coseismic elastic extension of the upper crust or by focusing of incoming seismic energy carried by direct body waves at depth.

We identified a possible precursory signal of the M4.7 earthquake. More investigations will be necessary to better understand the occurrence of precursory events of earthquakes. Mud volcanoes seem to be promising environments particularly sensitive to external perturbations. We suggest that mud systems could and should be used as natural laboratories to gain a better understanding of the physical processes underlying triggering dynamics.

ACKNOWLEDGEMENTS

The authors thanks Luciano Callegari and Marzia Conventi for their support in the logistics and their warm welcome. Sebastian Schoppohl is thanked for help in the field. Comments from an anonymous reviewer contributed to improve the paper. The authors would like to thank the editor Joachim Wassermann for providing insightful and constructive suggestions that strengthen the present manuscript.

REFERENCES

Accaino, F., Bratus, A., Conti, S., Fontana, D. & Tinivella, U., 2007. Fluid seepage in mud volcanoes of the northern apennines: an integrated geophysical and geological study, *J. appl. Geophys.,* **63**(2), 90–101.

Bessonova, E., Bortnikova, S., Gora, M., Manstein, Y.A., Shevko, A.Y., Panin, G. & Manstein, A., 2012. Geochemical and geo-electrical study of mud pools at the Mutnovsky volcano (South Kamchatka, Russia): behavior of elements, structures of feeding channels and a model of origin, *Appl. Geochem.,* **27**(9), 1829–1843.

Beyreuther, M., Barsch, R., Krischer, L., Megies, T., Behr, Y. & Wassermann, J., 2010. Obspy: a python toolbox for seismology, *Seismol. Res. Lett.,* **81**(3), 530–533.

Binley, A. & Kemna, A., 2005. DC resistivity and induced polarization methods, in *Hydrogeophysics,* pp. 129–156, eds Rubin, Y. & Hubbard, S.S., Springer.

Bonini, M., 2008. Elliptical mud volcano caldera as stress indicator in an active compressional setting (Nirano, Pede-Apennine margin, northern Italy), *Geology,* **36**(2), 131–134.

Bonini, M., 2009. Mud volcano eruptions and earthquakes in the Northern Apennines and Sicily, Italy, *Tectonophysics,* **474**(3), 723–735.

Bonini, M., 2012. Mud volcanoes: indicators of stress orientation and tectonic controls, *Earth-Sci. Rev.,* **115**(3), 121–152.

Caputo, R., Piscitelli, S., Oliveto, A., Rizzo, E. & Lapenna, V., 2003. The use of electrical resistivity tomographies in active tectonics: examples from the Tyrnavos Basin, Greece, *J. Geodyn.,* **36**(1), 19–35.

Chadha, R.K., Pandey, A.P. & Kuempel, H.J., 2003. Search for earthquake precursors in well water levels in a localized seismically active area of Reservoir Triggered Earthquakes in India, *Geophys. Res. Lett.,* **30**(7), 1416, doi:10.1029/2002GL016694.

Conrad, C.P., Bilek, S. & Lithgow-Bertelloni, C., 2004. Great earthquakes and slab pull: interaction between seismic coupling and plateslab coupling, *Earth planet. Sci. Lett.,* **218**(1–2), 109–122.

Crampin, S., Evans, R. & Atkinson, B.K., 1984. Earthquake prediction: a new physical basis, *Geophys. J. Int.,* **76**(1), 147–156.

Delle Donne, D., Harris, A., Ripepe, M. & Wright, R., 2010. Earthquake-induced thermal anomalies at active volcanoes, *Geology,* **38,** 771–774.

Farias, C., Lupi, M., Fuchs, F. & Miller, S.A., 2014. Seismic activity of the Nevados de Chillán volcanic complex after the 2010 Mw8.8 Maule, Chile, earthquake, *J. Volc. Geotherm. Res.,* **283**(0), 116–126.

Ferrazzini, V., Chouet, B., Fehler, M. & Aki, K., 1990. Quantitative analysis of long-period events recorded during hydrofracture experiments at Fenton Hill, New Mexico, *J. geophys. Res.,* **95**(B13), 21 871–21 884.

Frehner, M., 2014. Krauklis wave initiation in fluid-filled fractures by seismic body waves, *Geophysics,* **79**(1), T27–T35.

Frehner, M. & Schmalholz, S.M., 2010. Finite-element simulations of stoneley guided-wave reflection and scattering at the tips of fluid-filled fractures, *Geophysics,* **75**(2), T23–T36.

Guidoboni, E., 1989. *I Terremoti Prima del Mille in Italia e Nell'area Mediterranea,* SGA.

Hill, D.P. & Prejean, S.G., 2007. Dynamic triggering, in *Treatise on Geophysics,* vol. 4, pp. 257–292, ed. Kanamori, H., Elsevier, Amsterdam.

Istadi, B.P., Pramono, G.H., Sumintadireja, P. & Alam, S., 2009. Modeling study of growth and potential geohazard for LUSI mud volcano: East Java, Indonesia, *Mar. Pet. Geol.,* **26**(9), 1724–1739.

Iverson, R.M. *et al.*, 2006. Dynamics of seismogenic volcanic extrusion at Mount St Helens in 2004–05, *Nature,* **444**(7118), 439–443.

Jones, N.F., 2001. Pliny the Younger's Vesuvius "Letters" (6.16 and 6.20), in *The Classical World*, Vol. 95, No. 1, pp. 31–48, Johns Hopkins Univ. Press. doi:10.2307/4352621.

Kawakatsu, H. *et al.*, 2000. Aso94: Aso seismic observation with broadband instruments, *J. Volc. Geotherm. Res.,* **101**(1), 129–154.

Kedar, S., Kanamori, H. & Sturtevant, B., 1998. Bubble collapse as the source of tremor at Old Faithful Geyser, *J. geophys. Res.,* **103**(B10), 24 283–24 299.

Kemna, A., 2000. Tomographic inversion of complex resistivity: theory and application, *PhD thesis,* Ruhr University of Bochum.

Koestel, J., Kemna, A., Javaux, M., Binley, A. & Vereecken, H., 2008. Quantitative imaging of solute transport in an unsaturated and undisturbed soil monolith with 3-D ERT and TDR, *Water Resour. Res.,* **44**, W12411, doi:10.1029/2007WR006755.

Korneev, V.A., 2011. Krauklis wave in a stack of alternating fluid-elastic layers, *Geophysics,* **76**(6), N47–N53.

Lupi, M., Saenger, H., Fuchs, F. & Miller, S., 2013. Lusi mud eruption triggered by geometric focusing of seismic waves, *Nature Geosci.,* doi:10.1038/ngeo1884.

Lupi, M., Fuchs, F. & Pacheco, J.F., 2014. Fault reactivation due to the M 7.6 Nicoya earthquake at the Turrialba-Irazú volcanic complex, Costa Rica: effects of dynamic stress triggering, *Geophys. Res. Lett.,* **41**(12), 4142–4148.

Maksimov, G., Derov, A., Kashtan, B. & Lazarkov, M.Y., 2011. Estimation of hydro-fracture parameters by analysis of tube waves at vertical seismic profiling, *Acoust. Phys.,* **57**(4), 529–541.

Manga, M. & Bonini, M., 2012. Large historical eruptions at subaerial mud volcanoes, Italy, *Nat. Hazards Earth Syst. Sci.,* **12,** 3377–3386.

Manga, M., Brumm, M. & Rudolph, M.L., 2009. Earthquake triggering of mud volcanoes, *Mar. Pet. Geol.,* **26**(9), 1785–1798.

Martinelli, G. & Ferrari, G., 1991. Earthquake forerunners in a selected area of Northern Italy: recent developments in automatic geochemical monitoring, *Tectonophysics,* **193**(4), 397–410.

Mellors, R., Kilb, D., Aliyev, A., Gasanov, A. & Yetirmishli, G., 2007. Correlations between earthquakes and large mud volcano eruptions, *J. geophys. Res.,* **112**(B4), B04304, doi:10.1029/2006JB004489.

Neuberg, J., 2000. Characteristics and causes of shallow seismicity in andesite volcanoes, *Phil. Trans. R. Soc. Lond., A.,* **358**(1770), 1533–1546.

Nguyen, F., Garambois, S., Chardon, D., Hermitte, D., Bellier, O. & Jongmans, D., 2007. Subsurface electrical imaging of anisotropic formations affected by a slow active reverse fault, Provence, France, *J. appl. Geophys.,* **62**(4), 338–353.

Nguyen, F. *et al.*, 2009. Characterization of seawater intrusion using 2D electrical imaging, *Near Surf. Geophys.,* **7**(1303), 377–390.

Park, S.K., Johnston, M.J.S., Madden, T.R., Morgan, F.D. & Morrison, H.F., 1993. Electromagnetic precursors to earthquakes in the ULF band: a review of observations and mechanisms, *Rev. Geophys.,* **31**(2), 117–132.

Pondrelli, S., Salimbeni, S., Perfetti, P. & Danecek, P., 2012. Quick regional centroid moment tensor solutions for the Emilia 2012 (northern Italy) seismic sequence, *Ann. Geophys.,* **55**(4), 615–621.

Revil, A., Karaoulis, M., Johnson, T. & Kemna, A., 2012. Review: some low-frequency electrical methods for subsurface characterization and monitoring in hydrogeology, *Hydrogeol. J.,* **20**(4), 617–658.

Rice, J.R. & Rudnicki, J.W., 1979. Earthquake precursory effects due to pore fluid stabilization of a weakening fault zone, *J. geophys. Res.,* **84**(B5), 2177–2193.

Roeloffs, E.A., 1988. Hydrologic precursors to earthquakes: a review, *Pure appl. Geophys.,* **126**(2–4), 177–209.

Sammonds, P.R., Meredith, P.G. & Main, I.G., 1992. Role of pore fluids in the generation of seismic precursors to shear fracture, *Nature,* **359**(6392), 228–230.

Samsonov, S. *et al.*, 2013. Low magnitude earthquakes generating significant subsidence: the Lunigiana case study, in *AGU Fall Meeting*, Abstract #G31A-0936.

Singha, K., Day-Lewis, F.D., Johnson, T. & Slater, L.D., 2015. Advances in interpretation of subsurface processes with time-lapse electrical imaging, *Hydrol. Process.,* **29**(6), 1549–1576.

Skelton, A. *et al.*, 2014. Changes in groundwater chemistry before two consecutive earthquakes in Iceland, *Nature Geosci.,* **7**(10), 752–756.

Suski, B., Brocard, G., Authemayou, C., Muralles, B.C., Teyssier, C. & Holliger, K., 2010. Localization and characterization of an active fault in an urbanized area in central Guatemala by means of geoelectrical imaging, *Tectonophysics,* **480**(1), 88–98.

Vanneste, K., Verbeeck, K. & Petermans, T., 2008. Pseudo-3D imaging of a low-slip-rate, active normal fault using shallow geophysical methods: the Geleen fault in the Belgian Maas River valley, *Geophysics,* **73**(1), B1–B9.

Zeyen, H., Pessel, M., Ledésert, B., Hébert, R., Bartier, D., Sabin, M. & Lallemant, S., 2011. 3D electrical resistivity imaging of the near-surface structure of mud-volcano vents, *Tectonophysics,* **509**(3), 181–190.